2022 30th Mediterranean Conference on Control and Automation (MED)
June 28 - July 1, 2022. Athens, Greece

2022 30th Mediterranean Conference on Control and Automation (MED) | 978-1-6654-0673-4/22/$31.00 ©2022 IEEE | DOI: 10.1109/MED54222.2022.9837257

Overlapping Internal Boundary Control of Lane-free Automated Vehicle Traffic with State and Input Inclusion*

Milad Malekzadeh, Ioannis Papamichail, Markos Papageorgiou, *Life Fellow, IEEE*

***Abstract*— Lane-free vehicle driving has been recently proposed for connected automated vehicles. Lane-free traffic implies that incremental changes of the road width lead to corresponding incremental changes of the traffic flow capacity. Internal boundary control (IBC) was introduced to flexibly share the total road width and capacity among the two traffic directions of a highway in real-time, so as to maximize the cross-road infrastructure utilization. Centralized solutions, requiring information from the whole highway stretch under consideration, have already been proposed, which, however, may be problematic for long highways with respect to the required communications and physical system architecture in real-time operation. This paper introduces an overlapping decentralized control scheme for IBC of lane-free automated vehicle traffic, based on a contractible controller, which is designed in a decomposed way (per subsystem) for an extended system. Simulation investigations, involving a realistic highway stretch and demand scenario, demonstrate that the proposed decentralized regulator is similarly efficient as the centralized solutions.**

I. Introduction

Recurrent traffic congestion is a serious problem for most big cities around the globe, causing extensive delays, increased fuel consumption, excessive environmental pollution, and reduced traffic safety. Conventional traffic control measures are valuable [1], [2] and, in some cases, able to delay or even circumvent the onset of congestion. However, they are not always sufficient to tackle heavily congested traffic conditions. Gradually emerging and future groundbreaking vehicle automation and communication systems should be exploited to develop innovative solutions that can be applied to smart road infrastructures. Recently, there has been a massive effort by the industry and by several research institutions to develop and deploy a variety of vehicle automation and communication systems that are transforming the vehicle capabilities [3].

A novel paradigm for vehicular traffic, which is appropriate for high penetration rates of vehicles equipped with high levels of vehicle automation and communication systems, was recently launched by the TrafficFluid concept [4]. The TrafficFluid concept suggests: (1) lane-free traffic, whereby vehicles are not bound to fixed traffic lanes, as in conventional traffic; (2) vehicle nudging, whereby vehicles may exert a "nudging" effect on, i.e. influence the movement of vehicles in front of them. In this context, the internal boundary control (IBC) concept offers a promising and innovative control measure aiming to achieve an unprecedented exploitation of the available road infrastructure [5]. IBC relies on the fact that, in lane-free traffic, the road capacity may exhibit incremental changes in response to corresponding incremental changes of the road width. This is in contrast to lane-based traffic, where capacity changes may only occur if the road width is changed by a discrete number of lanes.

Consider a road with two opposite traffic directions serving connected automated vehicles (CAVs). The total cross-road capacity (for both directions) may be shared between the two directions in a flexible way, according to the prevailing demand per direction. Flexible capacity sharing may be achieved by virtually moving the internal boundary that separates the two traffic directions and communicating this decision to CAVs, so that they respect the road boundary. This way, the total capacity share assigned per direction can be changed in space and time according to an appropriate real-time control strategy (IBC), as illustrated in Fig. 1, in order to maximize the traffic efficiency of the overall system.

Sharing the total cross-road capacity among the two traffic directions is a control measure, known as tidal flow (or reversible lanes), that has been occasionally employed for conventional lane-based traffic, typically with manual interventions [6]. In order to deal with this problem, optimal control or feedback control algorithms of various types were proposed [7], [8].

Reversible lanes have also been considered for lane-based CAV traffic. The system-optimal dynamic traffic assignment models formulated in [9], using the Cell Transmission Model (CTM) [10] are utilized in [11]. Lanes are introduced as integer variables, and the problem is formulated as a mixed-integer linear programming problem that has exponential complexity.

The use of tidal flow control systems in lane-based traffic is not widespread for a number of reasons, including the harsh resolution of infrastructure sharing (only by lane quanta) among the two traffic directions; the serious counter-

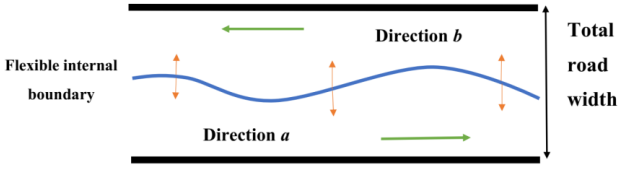

Figure 1. Space-time flexible internal road boundary in lane-free traffic.

* The research leading to these results has received funding from the European Research Council under the European Union's Horizon 2020 Programme / ERC Grant Agreement no. 833915, project TrafficFluid, see: https://www.trafficfluid.tuc.gr.

All authors are with the Dynamic Systems and Simulation Laboratory, Technical University of Crete, Chania 73100, Greece. M. Papageorgiou is also with the Faculty of Maritime and Transportation, Ningbo University, Ningbo, China.
(e-mails: mmalek@dssl.tuc.gr; ipapa@dssl.tuc.gr; markos@dssl.tuc.gr).

problems due to frequent merging or diverging traffic at lane-drop or lane-gain areas; and the safety-induced time-delays after each lane switch. These serious difficulties entail very limited capacity sharing flexibility in space and time and hinder reversible lane control from being a major traffic management measure. In contrast, in a lane-free CAV traffic environment, the mentioned difficulties are largely mitigated. More specifically, the resolution of road-width sharing among the two directions can be high; the smooth CAV driving on a lane-free road surface allows for the internal boundary to be a smooth space-function, as illustrated in Fig. 1; while assuming moderate changes of the internal boundary over time and space, the aforementioned safety-induced time-delay may be very small.

Thanks to these characteristics, real-time IBC for lane-free CAV traffic may be broadly applicable to the high number of arterial or highway infrastructures that feature unbalanced demands during the day in the two traffic directions, so as to strongly mitigate or even utterly avoid congestion. Even for infrastructures experiencing strong demand in both directions quasi-simultaneously, real-time IBC may intensify the road utilization and lead to sensible improvements.

The IBC problem is analyzed in [5], where its high improvement potential is demonstrated by formulating and solving an open-loop optimal control problem, in the form of a convex Quadratic Programming (QP) problem. That approach may be used within a Model Predictive Control (MPC) frame, with online demand prediction, for real-time application. However, simpler real-time approaches with similar efficiency, but without the need for online demand prediction, are preferable. This is why feedback-based Linear-Quadratic Regulators (LQR) were developed [12] for IBC and were demonstrated to be robust and similarly efficient as the open-loop optimal control solution, while avoiding the need for accurate modelling and external demand prediction. However, the centralized LQR may have to be designed with hundreds of state variables; also, it requires real-time information from the whole highway stretch under consideration, which may be problematic for very long highways with respect to the required communications and physical system architecture in real-time operation.

Several schemes have been suggested to realize decentralized control of interconnected systems [13], [14]. This paper develops a decentralized control scheme for IBC, based on a contractible controller developed for an extended model that exploits the overlapping structure of the system. The approach allows for a decomposed design of the controller, separately for each subsystem, which enhances scalability and expandability of the system. This approach was first introduced by Ikeda et al. [15] and was extended by İftar and Özgüner [16] to consider input inclusion, additionally to state inclusion. Simulation investigations, involving a realistic highway stretch and demand scenario, demonstrate that the proposed regulator is similarly efficient as the centralized LQR and the open-loop QP solution.

The well-known CTM is used, after linearization, for controller design; and, in its full nonlinear form, for simulation testing. The performance of the overlapping decentralized control scheme is compared to the no-control case. Section II presents some background issues and the appropriately adjusted CTM equations, while Section III presents the design of the decentralized regulator. Simulation investigations are discussed in Section IV, while conclusions are given in Section V.

II. BACKGROUND

Lane-free traffic is not expected to give rise to structural changes of existing macroscopic traffic flow models. As also supported by results in [4], notions and concepts like the conservation equation, the Fundamental Diagram (FD), as well as moving traffic waves will continue to characterize macroscopic traffic flow modelling in the case of lane-free automated vehicle traffic. Some IBC modelling background information, necessary for understanding the controller design and application, is repeated here for completeness. An extended version of CTM, a first-order dynamic traffic flow model with a triangular FD, will be considered.

Let us call the two opposite traffic directions, presented in Fig. 1, directions a (from left to right) and b (from right to left). The stretch is subdivided into n sections, with lengths L_i, $i=1,2,\ldots,n.$ The total road width (both directions) w, which is assumed constant over all sections for simplicity, can be flexibly shared between the two directions of each section in real-time. As a result, each direction is assigned a corresponding road width $w_i^a=\varepsilon_i\cdot w$ and $w_i^b=(1-\varepsilon_i)\cdot w,$ where $0\le\varepsilon_i\le 1$ is the sharing factor per section $i=1,2,\ldots,n,$ to be specified in real time as a control input by the internal boundary controller. The total section capacity q_{cap}, as well as the total critical density ρ_{cr} and the total jam density $\rho_{\max}$, are shared between the two traffic directions a and b. Based on the derivation presented in [5], these are given by

$$\begin{aligned} q_{i,cap}^a(\varepsilon_i)&=\varepsilon_i\cdot q_{cap},\ q_{i,cap}^b(\varepsilon_i)=(1-\varepsilon_i)\cdot q_{cap}\\ \rho_{i,cr}^a(\varepsilon_i)&=\varepsilon_i\cdot \rho_{cr},\ \rho_{i,cr}^b(\varepsilon_i)=(1-\varepsilon_i)\cdot \rho_{cr}\\ \rho_{i,\max}^a(\varepsilon_i)&=\varepsilon_i\cdot \rho_{\max},\ \rho_{i,\max}^b(\varepsilon_i)=(1-\varepsilon_i)\cdot \rho_{\max}\end{aligned} \tag{1}$$

For the IBC problem, we would like to disallow the complete closure of either direction; hence, the assigned road width in either direction should never be less than the widest vehicles driving on the road. This requirement gives rise to stricter constraints for the sharing factors as follows

$$0<\varepsilon_{i,\min}\le\varepsilon_i\le\varepsilon_{i,\max}<1 \tag{2}$$

where $\varepsilon_{i,\min}w$ and $(1-\varepsilon_{i,\max})w$ are the minimum admissible widths to be assigned to directions a and b, respectively.

Another restriction to be applied to the sharing factors concerns the time-delay needed to evacuate traffic on the direction that receives a restricted width, compared to the previous control time-step. This time-delay is small in lane-free CAV traffic without physical barrier among the two traffic directions and with moderate changes of the sharing

factors applied to short sections, but needs nevertheless to be considered. Clearly, the time-delay should apply only to the traffic direction that is being widened, compared to the previous control interval; while the direction that is restricted should promptly apply the smaller width, so that CAVs therein move out of the reduced-width zone. Assume that the required time-delay is smaller than or equal to the control time interval T_c; then, the time-delay requirement is automatically fulfilled for each section i, if the sharing factors that are actually applied to the two directions, i.e. ε_i^a and ε_i^b, respectively, are calculated as follows

$$\begin{aligned} \varepsilon_i^a(k_c) &= \min\{\varepsilon_i(k_c), \varepsilon_i(k_c-1)\} \\ \varepsilon_i^b(k_c) &= \min\{1-\varepsilon_i(k_c), 1-\varepsilon_i(k_c-1)\} \end{aligned} \tag{3}$$

where $k_c = 0,1,\ldots$ is the discrete control time index. It is noted that the notation $\varepsilon_i^a(k_c)$ and $\varepsilon_i^b(k_c)$ indicates that the sharing factors are applied for the duration of the control time interval $[k_c \cdot T_c, (k_c+1)\cdot T_c)$. The above equations may be readily extended if the required time-delay is a multiple of the control time interval T_c.

Traffic flows from section 1 to section n in direction a; and from section n to section 1 in direction b (see Fig. 2 as an example). We denote ρ_i^a, $i = 1,2,\ldots,n$, the traffic density of section i, direction a; and ρ_i^b, $i = 1,2,\ldots,n$, the traffic density of section i, direction b. Similarly, we denote q_i^a and q_i^b, $i = 1,2,\ldots,n$, the mainstream exit flows of section i for directions a and b, respectively. Thus, q_0^a is the feeding upstream mainstream inflow for direction a; and q_{n+1}^b is the feeding upstream mainstream inflow for direction b. Every section may have an on-ramp or an off-ramp at its upstream boundary. The on-ramp flows (if any) at section i are denoted r_i^a for direction a, and r_i^b for direction b. The off-ramp flow (if any) of section i, direction a, is calculated based on known exit rates β_i^a multiplied with the upstream-section flow, i.e. $\beta_i^a q_{i-1}^a$; and the off-ramp flow (if any) of section i, direction b, is calculated based on known exit rates β_i^b multiplied with the upstream-section flow, i.e. $\beta_i^b q_{i+1}^b$. The conservation equation for the section i of direction a is:

$$\rho_i^a(k+1) = \rho_i^a(k) + \frac{T}{L_i}((1-\beta_i^a)q_{i-1}^a(k) - q_i^a(k) + r_i^a(k)) \tag{4}$$

where T is the model time-step, typically set equal to 5–10 s for section lengths of some 500 m, and $k = 0,1,\ldots$ is the corresponding discrete-time index of the model.

According to CTM, traffic flow is obtained as the minimum of demand and supply functions, except for the last section, where only the demand function is considered, assuming that the downstream traffic conditions are uncongested. Considering the impact of the respective sharing factors on the FDs, we have

$$q_i^a(k) = \min\left\{Q_D(\rho_i^a(k), \varepsilon_i(k)), \frac{Q_S(\rho_{i+1}^a(k), \varepsilon_{i+1}(k))}{(1-\beta_{i+1}^a)} - r_{i+1}^a(k)\right\}, \quad i = 1,2,\ldots,n-1$$

$$q_n^a(k) = Q_D(\rho_n^a(k), \varepsilon_n(k)). \tag{5}$$

The demand and supply functions are given by the following respective equations

$$\begin{aligned} Q_D(\rho,\varepsilon) &= \min\{\varepsilon q_{cap}, v_f \rho\} \\ Q_S(\rho,\varepsilon) &= \min\{\varepsilon q_{cap}, w_s(\varepsilon\rho_{\max} - \rho)\} \end{aligned} \tag{6}$$

where v_f is the free speed (which is assumed equal for all sections for simplicity) and w_s is the back-wave speed.

The equations for section i of direction b are analogous to those of direction a, with few necessary index modifications. Section numbers in direction b are descending, hence we have

$$\rho_i^b(k+1) = \rho_i^b(k) + \frac{T}{L_i}((1-\beta_i^b)q_{i+1}^b(k) - q_i^b(k) + r_i^b(k)) \tag{7}$$

and the flows are given by

$$\begin{aligned} q_1^b(k) &= Q_D(\rho_1^b(k), (1-\varepsilon_1(k))) \\ q_i^b(k) &= \min\left\{Q_D(\rho_i^b(k), (1-\varepsilon_i(k))), \frac{Q_S(\rho_{i-1}^b(k), (1-\varepsilon_{i-1}(k)))}{(1-\beta_{i-1}^b)} - r_{i-1}^b(k)\right\}, i = 2,3,\ldots,n \end{aligned} \tag{8}$$

In conventional traffic management, traffic densities characterize clearly the state of traffic, depending on their value versus the critical density: free traffic (when density is lower than critical density), critical traffic (when density is around critical density) or congested traffic (when density is higher than critical density). However, in the proposed scheme, the critical density for each direction and section is not constant, but a function of the sharing factor (see (1)), and is changing according to the applied control action. Therefore, the density value by itself is not sufficient, in the IBC context, to characterize the traffic situation in a section.

To address this issue, the following relations define the relative densities (dimensionless) per section and per direction. The relative density of section i and direction a or b is obtained by dividing the corresponding traffic density with the corresponding critical density, which, on its turn, depends (via (1)) on the sharing factor prevailing during the last time-step. Thus we have

$$\tilde{\rho}_i^a(k) = \frac{\rho_i^a(k)}{\varepsilon_i(k-1)\rho_{cr}}, \quad \tilde{\rho}_i^b(k) = \frac{\rho_i^b(k)}{(1-\varepsilon_i(k-1))\rho_{cr}}. \tag{9}$$

The relative densities reflect clearly the state of the traffic in the IBC context. Specifically, if the relative density of a section and direction is less than 1, it reflects under-critical (free-flow) traffic conditions; if it is around 1, it reflects capacity flow; and if it is greater than 1, it reflects over-critical (congested) traffic conditions.

Linearization of the above system of dynamic equations around a nominal point was presented analytically in [12]. To achieve this, the one-step retarded control input has to be defined as a new state variable according to

$\gamma_i(k+1) = \varepsilon_i(k), \quad i = 1,2,\ldots,n.$ Following the same linearization procedure as in [12], the linearized state-space model is

$$\mathbf{x}(k+1) = \hat{\mathbf{A}}\mathbf{x}(k) + \hat{\mathbf{B}}\mathbf{u}(k) \tag{10}$$

where $\mathbf{x}(k) = [\Delta\tilde{\rho}_1^a(k), \Delta\tilde{\rho}_1^b(k), \Delta\gamma_1(k), \ldots, \Delta\tilde{\rho}_n^a(k), \Delta\tilde{\rho}_n^b(k), \Delta\gamma_n(k)]^T$ is the state vector and $\mathbf{u}(k) = \boldsymbol{\Delta\varepsilon}(k)$ is the control vector, whereby $\boldsymbol{\Delta\varepsilon}(k) = [\Delta\varepsilon_1(k), \ldots, \Delta\varepsilon_n(k)]^T$. Also, $\Delta(.)(k) = (.)(k) - (.)^N$, the superscript N denoting the nominal values, while it has been assumed that $\Delta(.)(k) = 0$ for all disturbances (upstream mainstream demands, as well as the on-ramp flows of each direction). $\hat{\mathbf{A}} \in \mathbb{R}^{3n\times 3n}$ and $\hat{\mathbf{B}} \in \mathbb{R}^{3n\times n}$ are the time-invariant state and input matrices, respectively, while $\mathbf{x} \in \mathbb{R}^{3n}$ and $\mathbf{u} \in \mathbb{R}^n$.

If the control time-step is defined as a multiple of the model time-step, i.e. $T_c = MT$, where M is an integer, then the discrete control time index is $k_c = \lfloor kT/T_c \rfloor$. Thus, the linear state-space equation may be changed as follows, in order to be based on the control time-step T_c,

$$\varphi: \mathbf{x}(k_c+1) = \mathbf{A}\mathbf{x}(k_c) + \mathbf{B}\mathbf{u}(k_c) \tag{11}$$

where $\mathbf{A} = \hat{\mathbf{A}}^M$, and $\mathbf{B} = (\hat{\mathbf{A}}^{M-1} + \hat{\mathbf{A}}^{M-2} + ... + \mathbf{I})\hat{\mathbf{B}}$.

When employing the LQR methodology as in [12], the control goal is the minimization of the quadratic criterion

$$J = \frac{1}{2}\sum_{k_c=0}^{\infty}\left[\left\|\mathbf{x}(k_c)\right\|_{\mathbf{Q}}^2 + \left\|\mathbf{u}(k_c)\right\|_{\mathbf{R}}^2\right] \tag{12}$$

where $\mathbf{Q} \in \mathbb{R}^{3n\times 3n}$ and $\mathbf{R} \in \mathbb{R}^{n\times n}$ are symmetric positive definite matrices. The first term penalizes deviations of the elements of the state variable from zero, i.e. deviations of $\tilde{\rho}_i^a(k_c)$, $\tilde{\rho}_i^b(k_c)$, $\gamma_i(k_c)$, $i = 1,2,\ldots,n,$ from their respective desired nominal values. The second term penalizes deviations of the control inputs from the nominal values.

The nominal value of relative densities is set equal to 1, so that the controller is motivated to operate the system near capacity, which is good for traffic efficiency. In addition, if capacity flow is not feasible (due to lack of demand or due to excessive demand), then minimizing a sum of squares has the tendency to balance deviations from the nominal values, something that is conform with the secondary operational sub-objective of balancing the margin to capacity across sections. On the other hand, we set to 0.5 the nominal value for the sharing factors, because minimization of the second term in (12) will mitigate deviations of the sharing factors from 0.5 and will balance these deviations in space and time, which are also secondary operational sub-objectives.

The optimal controller minimizing the criterion (11) subject to the model (10) is given by a linear feedback control law of the form $\mathbf{u}(k_c) = \mathbf{K}\mathbf{x}(k_c)$, where $\mathbf{K} \in \mathbb{R}^{n\times 3n}$ is a constant gain matrix given by

$$\mathbf{K} = (\mathbf{R} + \mathbf{B}^T\mathbf{P}\mathbf{B})^{-1}\mathbf{B}^T\mathbf{P}\mathbf{A} \tag{13}$$

and $\mathbf{P}$ is a unique positive semidefinite solution of the discrete-time algebraic Riccati equation.

III. Overlapping Control Scheme with State and Input Inclusion

Summarizing from above, each highway section has three state variables and one control input, which is the corresponding sharing factor. For very long highways, the centralized LQR, proposed in [12] and outlined above, calls for the solution of an accordingly large-scale Riccati equation. More importantly, the centralized LQR requires real-time information for all the states of the system to compute each control input. This requirement may be problematic for long highways due to the need to transfer data from the whole highway in order to compute each sharing factor. In addition, traffic conditions on a long highway are usually inhomogeneous, i.e. they may be simultaneously free-flowing or critical or congested at different highway parts. In such circumstances, the mentioned balancing of relative density and sharing factor deviations from their respective nominal values may not be fully appropriate when applied to all sections of the long highway, due to strong differences in the prevailing traffic conditions.

For the above reasons, there is an interest in developing a decentralized control scheme, which may: reduce the LQR design complexity; enhance the extendibility to new parts of a highway, without the need for re-designing the whole approach; reduce the burden of real-time data transferring; and handle locally the balancing of variable deviations from their nominal values. Due to strong dependencies between consecutive sections in IBC, developing a fully decentralized control scheme may reduce the control efficiency compared to the centralized case, as was indeed confirmed in preliminary investigations.

Therefore, in this study, an overlapping control strategy is proposed. The approach relies on the separation of the highway into a number of subsequent subsystems (highway stretches) which are overlapping, i.e. adjacent subsystems have some sections in common; hence, adjacent subsystems share some states and some control inputs. This approach delivers overlapping decentralized controllers, where, thanks to the overlapping structure, subsystems remain aware about the inter-relations with adjacent subsystems.

The control inputs of the non-overlapping sections use only local subsystem information; while control inputs in the overlapping sections use information from both adjacent subsystems. In order to develop this control scheme, some transformations must be applied to the original system to create an expanded system. This procedure is presented next.

Consider the following linear time-invariant system

$$\tilde{\varphi}: \ \tilde{\mathbf{x}}(k_c+1) = \tilde{\mathbf{A}}\tilde{\mathbf{x}}(k_c) + \tilde{\mathbf{B}}\tilde{\mathbf{u}}(k_c) \tag{14}$$

where $\tilde{\mathbf{x}} \in \mathbb{R}^{\tilde{n}}$ and $\tilde{\mathbf{u}} \in \mathbb{R}^{\tilde{m}}$. In the following, the system φ in (11) is referred to as the original system, and $\tilde{\varphi}$ is referred to as the expanded system. It is assumed that $\tilde{n} \geq 3n$ and $\tilde{m} \geq n$, as the expanded system $\tilde{\varphi}$ has typically more states and more inputs than the original system φ due to the expansion. More specifically, the goal of the expansion is to

create overlapping areas that belong to both corresponding adjacent subsystems, and this leads to higher state and control dimensions for the expanded system.

The state and the input of the original system are partitioned as

$$\begin{aligned} \mathbf{x} &= (\mathbf{x}_1^T, \mathbf{x}_2^T, \ldots, \mathbf{x}_P^T), \quad \mathbf{x}_i \in \mathbb{R}^{n_i} \\ \mathbf{u} &= (\mathbf{u}_1^T, \mathbf{u}_2^T, \ldots, \mathbf{u}_P^T), \quad \mathbf{u}_i \in \mathbb{R}^{m_i} \end{aligned} \tag{15}$$

where $P \geq 3$ is the odd number of partitions (subsequent highway stretches). Here it is assumed that, for all even indexes i, $\mathbf{x}_i$ and $\mathbf{u}_i$ correspond to the overlapping parts of the state and input vectors, respectively, while for all odd indexes i, $\mathbf{x}_i$ and $\mathbf{u}_i$ correspond to the non-overlapping parts of the state and input spaces.

Now consider that the matrices $\mathbf{A}$ and $\mathbf{B}$ for the system φ are also partitioned compatibly, as follows:

$$\begin{bmatrix} \mathbf{A}_{11} & \mathbf{A}_{12} & \cdots & \mathbf{A}_{1P} \\ \mathbf{A}_{21} & \mathbf{A}_{22} & \cdots & \mathbf{A}_{2P} \\ \vdots & \vdots & \ddots & \vdots \\ \mathbf{A}_{P1} & \mathbf{A}_{P2} & \cdots & \mathbf{A}_{PP} \end{bmatrix}, \begin{bmatrix} \mathbf{B}_{11} & \mathbf{B}_{12} & \cdots & \mathbf{B}_{1P} \\ \mathbf{B}_{21} & \mathbf{B}_{22} & \cdots & \mathbf{B}_{2P} \\ \vdots & \vdots & \ddots & \vdots \\ \mathbf{B}_{P1} & \mathbf{B}_{P2} & \cdots & \mathbf{B}_{PP} \end{bmatrix}. \tag{16}$$

Note that an expanded system $\tilde{\varphi}$ can be obtained from the original system φ if it satisfies certain conditions presented in [16]; and such an extension can be leveraged in order to design the controller for the original system based on the design of a controller for the extended system. For the case of overlapping areas belonging to exactly two corresponding adjacent subsystems, as in the IBC application, the extended system matrices $\tilde{\mathbf{A}}$ and $\tilde{\mathbf{B}}$ can be easily obtained from the original matrices $\mathbf{A}$ and $\mathbf{B}$ by simply doubling the state equations of the overlapping partitions. This expansion may be readily shown to satisfy the conditions required in [16] for an extension of the original system.

As an example, the system considered in the following investigations (see Fig. 2) may be separated in two subsystems with a single overlapping area of two sections, i.e. based on three partitions ($P = 3$) of the original system. As can be seen in Fig. 2, we consider two subsystems with six sections each; while sections 5 and 6 are taken into account as an overlapping area. The two subsystems are strongly connected through the overlapping area. The matrices for the extended system with $P = 3$ are obtained by doubling the state equations of the overlapping sections:

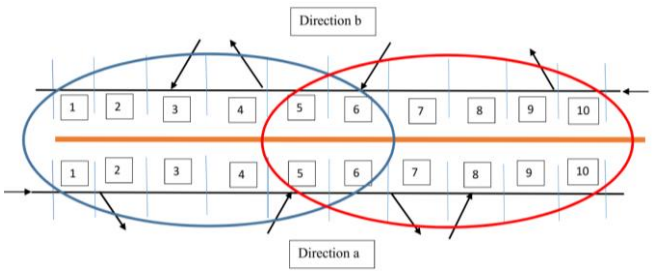

Figure 2. The considered highway stretch.

$$\tilde{\mathbf{A}} = \left[\begin{array}{cc:cc} \mathbf{A}_{11} & \mathbf{A}_{12} & 0 & \mathbf{A}_{13} \\ \mathbf{A}_{21} & \mathbf{A}_{22} & 0 & \mathbf{A}_{23} \\ \hdashline \mathbf{A}_{21} & 0 & \mathbf{A}_{22} & \mathbf{A}_{23} \\ \mathbf{A}_{31} & 0 & \mathbf{A}_{32} & \mathbf{A}_{33} \end{array}\right] \triangleq \begin{bmatrix} \tilde{\mathbf{A}}_1 & \tilde{\mathbf{A}}_{12} \\ \tilde{\mathbf{A}}_{21} & \tilde{\mathbf{A}}_2 \end{bmatrix} \tag{17}$$

$$\tilde{\mathbf{B}} = \left[\begin{array}{cc:cc} \mathbf{B}_{11} & \mathbf{B}_{12} & \mathbf{B}_{12} & \mathbf{B}_{13} \\ \mathbf{B}_{21} & \mathbf{B}_{22} & \mathbf{B}_{22} & \mathbf{B}_{23} \\ \hdashline \mathbf{B}_{21} & \mathbf{B}_{22} & \mathbf{B}_{22} & \mathbf{B}_{23} \\ \mathbf{B}_{31} & \mathbf{B}_{32} & \mathbf{B}_{32} & \mathbf{B}_{33} \end{array}\right] \triangleq \begin{bmatrix} \tilde{\mathbf{B}}_1 & \tilde{\mathbf{B}}_{12} \\ \tilde{\mathbf{B}}_{21} & \tilde{\mathbf{B}}_2 \end{bmatrix} \tag{18}$$

Note that in the specific IBC application, the non-zero coupling matrices $\tilde{\mathbf{A}}_{12}$, $\tilde{\mathbf{A}}_{21}$, $\tilde{\mathbf{B}}_{12}$ and $\tilde{\mathbf{B}}_{21}$ have most of their elements equal to zero.

For the general case, consider $n_D = (P+1)/2$ decoupled subsystems:

$$\varphi_i^D : \tilde{\mathbf{x}}_i(k_c+1) = \tilde{\mathbf{A}}_i \tilde{\mathbf{x}}_i(k_c) + \tilde{\mathbf{B}}_i \tilde{\mathbf{u}}_i(k_c), \; i = 1, \ldots n_D \tag{19}$$

where

$$\begin{aligned} \tilde{\mathbf{A}}_1 &= \begin{bmatrix} \mathbf{A}_{11} & \mathbf{A}_{12} \\ \mathbf{A}_{21} & \mathbf{A}_{22} \end{bmatrix}, \quad \tilde{\mathbf{A}}_{n_D} = \begin{bmatrix} \mathbf{A}_{(P-1)(P-1)} & \mathbf{A}_{(P-1)P} \\ \mathbf{A}_{P(P-1)} & \mathbf{A}_{PP} \end{bmatrix}, \\ \tilde{\mathbf{A}}_i &= \begin{bmatrix} \mathbf{A}_{(2i-2)(2i-2)} & \mathbf{A}_{(2i-2)(2i-1)} & \mathbf{A}_{(2i-2)(2i)} \\ \mathbf{A}_{(2i-1)(2i-2)} & \mathbf{A}_{(2i-1)(2i-1)} & \mathbf{A}_{(2i-1)(2i)} \\ \mathbf{A}_{(2i)(2i-2)} & \mathbf{A}_{(2i)(2i-1)} & \mathbf{A}_{(2i)(2i)} \end{bmatrix}, i = 2, \ldots, n_D - 1 \end{aligned} \tag{20}$$

and

$$\begin{aligned} \tilde{\mathbf{B}}_1 &= \begin{bmatrix} \mathbf{B}_{11} & \mathbf{B}_{12} \\ \mathbf{B}_{21} & \mathbf{B}_{22} \end{bmatrix}, \tilde{\mathbf{B}}_{n_D} = \begin{bmatrix} \mathbf{B}_{(P-1)(P-1)} & \mathbf{B}_{(P-1)P} \\ \mathbf{B}_{P(P-1)} & \mathbf{B}_{PP} \end{bmatrix}, \\ \tilde{\mathbf{B}}_i &= \begin{bmatrix} \mathbf{B}_{(2i-2)(2i-2)} & \mathbf{B}_{(2i-2)(2i-1)} & \mathbf{B}_{(2i-2)(2i)} \\ \mathbf{B}_{(2i-1)(2i-2)} & \mathbf{B}_{(2i-1)(2i-1)} & \mathbf{B}_{(2i-1)(2i)} \\ \mathbf{B}_{(2i)(2i-2)} & \mathbf{B}_{(2i)(2i-1)} & \mathbf{B}_{(2i)(2i)} \end{bmatrix}, i = 2, \ldots, n_D - 1 \end{aligned} \tag{21}$$

We can now calculate the gains for the feedback law for each decoupled subsystem $\tilde{\mathbf{u}}_i(k_c) = \tilde{\mathbf{K}}^i \tilde{\mathbf{x}}_i(k_c)$ using the LQR method for objectives similar to (12). If the resulting subsystem gains $\tilde{\mathbf{K}}^i$ are partitioned as follows:

$$\begin{aligned} \tilde{\mathbf{K}}^i &= \begin{bmatrix} \tilde{\mathbf{K}}_{11}^i & \tilde{\mathbf{K}}_{12}^i \\ \tilde{\mathbf{K}}_{21}^i & \tilde{\mathbf{K}}_{22}^i \end{bmatrix}, \quad i = 1, n_D \\ \tilde{\mathbf{K}}^i &= \begin{bmatrix} \tilde{\mathbf{K}}_{11}^i & \tilde{\mathbf{K}}_{12}^i & \tilde{\mathbf{K}}_{13}^i \\ \tilde{\mathbf{K}}_{21}^i & \tilde{\mathbf{K}}_{22}^i & \tilde{\mathbf{K}}_{23}^i \\ \tilde{\mathbf{K}}_{31}^i & \tilde{\mathbf{K}}_{32}^i & \tilde{\mathbf{K}}_{33}^i \end{bmatrix}, \quad i = 2, \ldots, n_D - 1 \end{aligned} \tag{22}$$

then the overall gain for the feedback control law of the extended system $\tilde{\mathbf{u}}(k_c) = \tilde{\mathbf{K}}\tilde{\mathbf{x}}(k_c)$ is given by

$$\tilde{\mathbf{K}} = \text{blockdiag}(\tilde{\mathbf{K}}^1, \ldots, \tilde{\mathbf{K}}^{n_D}). \tag{23}$$

Based on [16], if $\tilde{\varphi}$ is an extension of φ, then the gain value $\mathbf{K}$ for the equivalent feedback control law of the original system, i.e. $\mathbf{u}(k_c) = \mathbf{K}\mathbf{x}(k_c)$, can be constructed using the gain value $\tilde{\mathbf{K}}$ from the feedback law of the ex-

tended system $\tilde{\mathbf{u}}(k_c) = \tilde{\mathbf{K}}\tilde{\mathbf{x}}(k_c)$. For the case of the overlapping systems considered here, the gain is as follows:

$$\mathbf{K} = \begin{bmatrix} \tilde{\mathbf{K}}_{11}^1 & \tilde{\mathbf{K}}_{12}^1 & 0 & 0 & 0 & 0 & \cdots & 0 \\ \tilde{\mathbf{K}}_{21}^1 & \tilde{\mathbf{K}}_{22}^1 + \tilde{\mathbf{K}}_{11}^2 & \tilde{\mathbf{K}}_{12}^2 & \tilde{\mathbf{K}}_{13}^2 & 0 & 0 & \cdots & 0 \\ 0 & \tilde{\mathbf{K}}_{21}^2 & \tilde{\mathbf{K}}_{22}^2 & \tilde{\mathbf{K}}_{23}^2 & 0 & 0 & \cdots & 0 \\ 0 & \tilde{\mathbf{K}}_{31}^2 & \tilde{\mathbf{K}}_{32}^2 & \tilde{\mathbf{K}}_{33}^2 + \tilde{\mathbf{K}}_{11}^3 & \tilde{\mathbf{K}}_{12}^3 & \tilde{\mathbf{K}}_{13}^3 & \cdots & 0 \\ 0 & 0 & 0 & \tilde{\mathbf{K}}_{21}^3 & \tilde{\mathbf{K}}_{22}^3 & \tilde{\mathbf{K}}_{23}^3 & \cdots & 0 \\ 0 & 0 & 0 & \tilde{\mathbf{K}}_{31}^3 & \tilde{\mathbf{K}}_{32}^3 & \tilde{\mathbf{K}}_{33}^3 + \tilde{\mathbf{K}}_{11}^4 & \cdots & 0 \\ \vdots & \vdots & \vdots & \vdots & \vdots & \vdots & \ddots & \vdots \\ 0 & 0 & 0 & 0 & 0 & 0 & \cdots & \tilde{\mathbf{K}}_{22}^{n_D} \end{bmatrix}. \quad (24)$$

and for the specific case of two subsystems:

$$\mathbf{K} = \begin{bmatrix} \tilde{\mathbf{K}}_{11}^1 & \tilde{\mathbf{K}}_{12}^1 & 0 \\ \tilde{\mathbf{K}}_{21}^1 & \tilde{\mathbf{K}}_{22}^1 + \tilde{\mathbf{K}}_{11}^2 & \tilde{\mathbf{K}}_{12}^2 \\ 0 & \tilde{\mathbf{K}}_{21}^2 & \tilde{\mathbf{K}}_{22}^2 \end{bmatrix}. \quad (25)$$

It is evident that the decoupled systems cannot capture fully the dynamics of the extended system due to ignoring of the weak interconnections among subsystems. Therefore, the proposed decentralized overlapping controller will be sub-optimal compared to the centralized LQR control approach.

In summary, the proposed design procedure for the present IBC application comprises:

- design of decoupled LQR controllers for each subsystem;
- computation of the control inputs of overlapping sections by the summation of the control inputs calculated by the distributed controllers for the two adjacent overlapping subsystems.

IV. Simulation Investigation

A. Simulation set-up

The considered highway stretch of Fig. 2 has a length of 5 km and is subdivided in 10 sections of 0.5 km each. The modelling time-step, T, is set to 10 s, and the considered time horizon is 1 h. While a linearization of CTM was used for LQR controller design, the full nonlinear CTM is used to represent the emulated ground truth in this section. The model parameters used in the simulation are $v_f = 100$ km/h and $w_s = 12$ km/h; while the total cross-road capacity to be shared among the two directions is $q_{cap} = 12{,}000$ veh/h. The exit rates for the four off-ramps are all set equal to 0.1. The mainstream and on-ramp demand flows per direction are presented in Fig. 3. It may be seen that the two directions feature respective peaks in their mainstream demands that are slightly overlapping.

The simulation results of the no-control case are presented first, followed by the results obtained when using the overlapping decentralized control scheme.

B. No-control case

When no IBC is applied, the total width of the highway stretch is equally shared by the two directions, i.e. the sharing factors ε_i are constant and equal to 0.5 for all sections. Using the demand profiles presented in Fig. 3 in the nonlinear CTM model with $\varepsilon_i = 0.5$, we get the simulation results

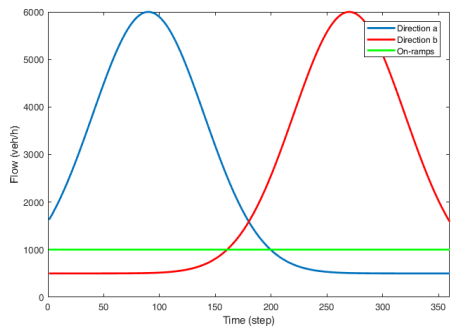

Figure 3. Demand flows per direction and on-ramp.

for the no-control case. Figure 4 displays the corresponding spatio-temporal evolution of the relative density defined in (9). According to the definition, relative density values lower than 1 refer to uncongested traffic; while values higher than 1 refer to congested traffic; when the relative density equals 1, and the downstream section is uncongested, we have capacity flow at the corresponding section.

Figure 4 shows that congestion is created in sections 5 and 8 for direction a due to the increased mainstream demand, in combination with the ramp inflows, at around $k = 70$. The congestion dissolves at around $k = 160$, due to the rapid decrease of the mainstream demand for this direction. In direction b, we have also congestion being triggered in sections 3 and 6 for similar reasons, at around $k = 240$. The congestion dissolves at around $k = 340$. The Total Time Spent by all vehicles in the highway stretch (TTS) is equal to 314.6 veh·h.

C. Control case

In order to apply the overlapping feedback regulators, as explained in Section III, we need to calculate offline the static gain matrices $\tilde{\mathbf{K}}^i$, $i = 1, 2$. A nominal point of operation is first selected for the calculation of the matrices $\hat{\mathbf{A}}$ and $\hat{\mathbf{B}}$ used in the linear model (11). The nominal values are $q_0^a\big|_N = q_{11}^b\big|_N = 5000$ veh/h, $r_5^a\big|_N = r_8^a\big|_N = r_3^b\big|_N = r_6^b\big|_N = 1000$ veh/h, $\tilde{\rho}_i^a\big|_N = \tilde{\rho}_i^b\big|_N = 1$ and $\varepsilon_i\big|_N = 0.5$, $i = 1, 2, \ldots, 10$. The control time-step, T_c, is set to 60 s, hence $M = 6$.

The regulators are operated in a closed-loop mode, receiving in emulated real time the respective section density values per direction from the CTM model equations; and responding with the sharing factors calculated. The sharing factors applied for the sections of the overlapping area are

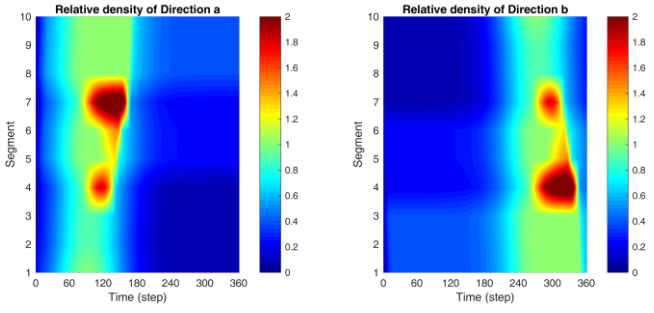

Figure 4. Relative density for the two directions in the no-control case.

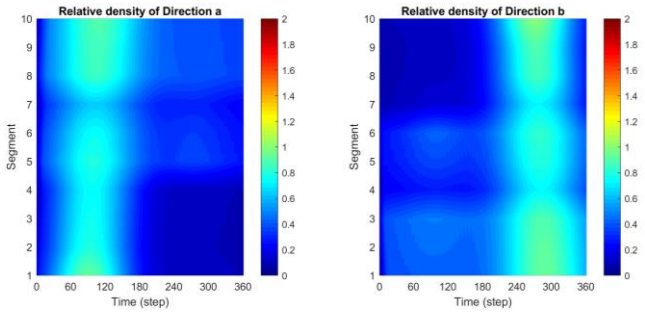

Figure 5. Relative density for the two directions in the control case.

given from the summation of the values calculated by the two separate regulators. The upper and lower bounds for the sharing factors, used to avoid utter blocking of any of the two directions, are equal for all sections $i = 1, 2, \ldots, 10$ and are given the values $\varepsilon_{i,\min} = 0.16$ and $\varepsilon_{i,\max} = 0.84$. This is repeated every $T_c = 60\,\text{s}$.

The resulting traffic conditions are under-critical everywhere as shown in the spatio-temporal evolution of the relative densities depicted in Fig. 5. More detailed information is presented in Figs. 6-10. Each figure has two columns reflecting the results of two respective sections; for each section (column), we provide three diagrams (rows):

- The first diagram shows the two traffic densities (in veh/km), for directions a and b, and the corresponding critical densities, which are changing according to the sharing factor in the section.
- The second diagram shows the two traffic flows, for directions a and b, and the corresponding capacities, which are changing according to the sharing factor in the section. In addition, the sum of both flows is also displayed.
- The third diagram shows the value of the control input, i.e. the sharing factor applied, as well as the constant bounds (black curves), which may lead to possible truncation of the control input.

The displayed results confirm that densities (flows) are always lower than the respective critical densities (capacities) in all sections and in both directions; hence traffic conditions are always under-critical for the whole stretch. In fact, the total-flow curve (for both directions) does not reach the total road capacity (of 12,000 veh/h) at any time anywhere. In short, congestion is utterly avoided and any occurring delays in the no-control case do not exist anymore.

The sharing factor trajectories for each section show that this excellent outcome is enabled via a smooth swapping of assigned capacity to the two directions, whereby more capacity is assigned to direction a during the first half of the time horizon and vice-versa for the second half, in response to the traffic (density) changes caused by the changing respective demands and their peaks. It is interesting to notice that the value of the control input is never saturated.

The achieved TTS value is 288.9 veh·h, indicating an improvement of 8.2% over the no-control case. The TTS

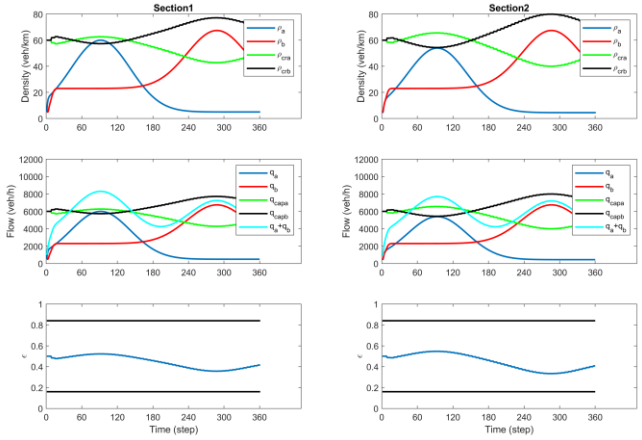

Figure 6. Density, flow and control trajectories in the control case (sections 1 and 2)

value obtained using the overlapping decentralized control scheme is, in fact, equal to the value that is achieved when applying the optimal control resulting from the QP problem formulation or the LQR formulation presented by the authors in [5] and [12], respectively. Thus, despite the use of a decentralized control scheme, where no demand predictions are necessary and the need for data communication is reduced, the proposed approach achieves the highest possible efficiency for the investigated scenario.

V. Conclusion

The concept of internal boundary control, introduced in [5], has been revisited in this study by use of a different feedback control approach with overlapping structure. The well-known CTM, appropriately adjusted to introduce the effect of the sharing factors, has been utilized for the development of the overlapping decentralized regulator for the IBC problem. An overlapping decentralized control design method [16] was adopted, which is based on a contractible controller developed for an extended system.

According to the IBC concept, the total road width and capacity are shared in each section in real-time among the two directions of the road in response to the prevailing traffic conditions. The overlapping regulator is easy to design, featuring lower complexity compared to the full-scale regulator; while its implementation reduces the communication requirements, which is beneficial in case of long highways.

Simulation investigations demonstrate that the overlapping decentralized control scheme is as efficient as an open-loop optimal control solution (with perfect model knowledge and demand prediction) developed for the same problem in [5] using a convex QP problem formulation; and as efficient as the centralized LQR formulation presented in [12].

Ongoing work considers application of the method on longer highway stretches as well as microscopic simulation studies with vehicles moving in a lane-free mode, based on appropriate CAV movement strategies that have been developed in the frame of the Trafficfluid project [4], [18].

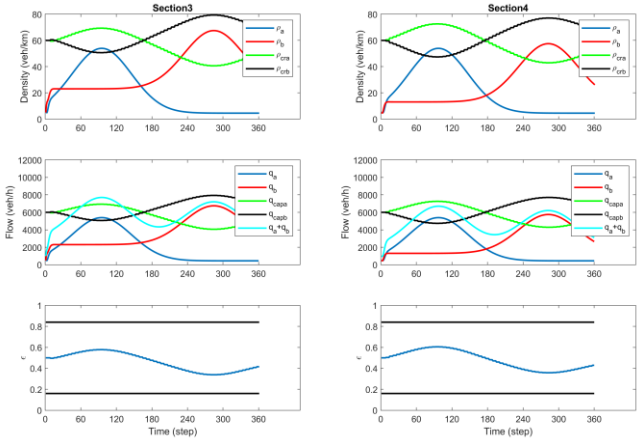

Figure 7. Density, flow and control trajectories in the control case (sections 3 and 4).

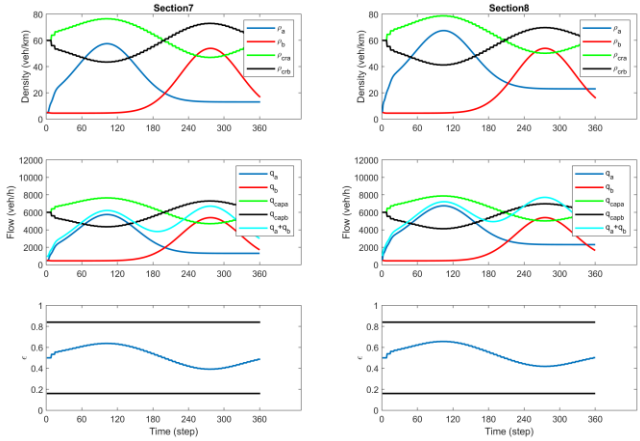

Figure 9. Density, flow and control trajectories in the control case (sections 7 and 8).

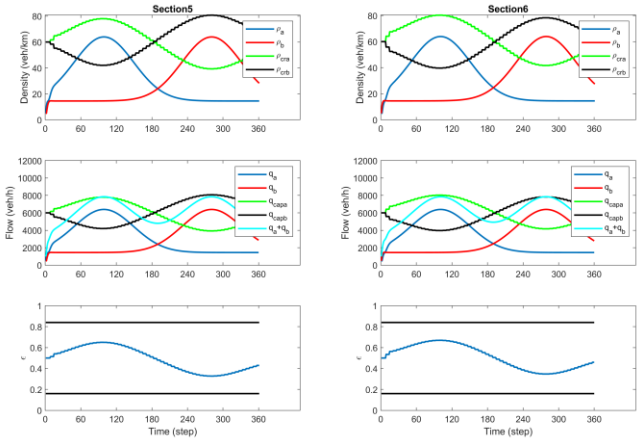

Figure 8. Density, flow and control trajectories in the control case (sections 5 and 6).

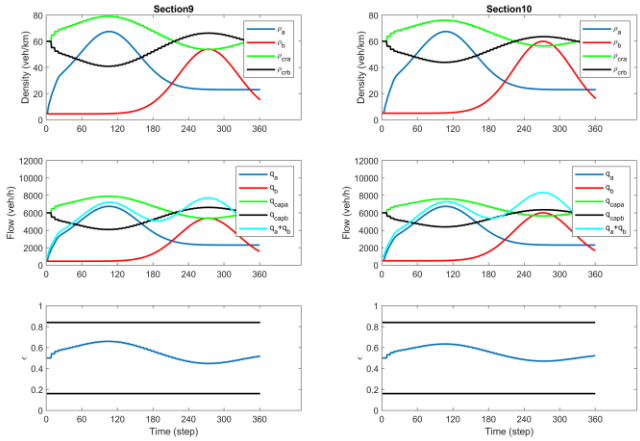

Figure 10. Density, flow and control trajectories in the control case (sections 9 and 10).

REFERENCES

[1] M. Papageorgiou, C. Diakaki, V. Dinopoulou, A. Kotsialos, and Y. Wang, "Review of road traffic control strategies," *Proceedings of the IEEE*, vol. 91, no. 12, pp. 2043–2067, 2003.

[2] A. A. Kurzhanskiy, and P. Varaiya, "Active traffic management on road networks: a macroscopic approach," *Philosophical Trans. of the Royal Society A: Mathematical, Physical and Engineering Sciences*, vol. 368, no. 1928, pp. 4607–4626, 2010.

[3] C. Diakaki, M. Papageorgiou, I. Papamichail, and I. Nikolos, "Overview and analysis of vehicle automation and communication systems from a motorway traffic management perspective," *Transp. Research Part A: Policy and Practice*, vol. 75, pp. 147–165, 2015.

[4] M. Papageorgiou, K. S. Mountakis, I. Karafyllis, I. Papamichail, and Y. Wang, "Lane-free artificial-fluid concept for vehicular traffic," *Proceeding of the IEEE*, vol. 109, pp. 114–121, 2021.

[5] M. Malekzadeh, I. Papamichail, M. Papageorgiou, and K. Bogenberger, "Optimal internal boundary control of lane-free automated vehicle traffic," *Transp. Research Part C*, vol. 126, 103060, 2021.

[6] B. Wolshon, and L. Lambert, "Reversible lane systems: Synthesis of practice," *Journal of Transp. Engineering*, vol. 132, no. 12, pp. 933–944, 2006.

[7] J. R. D. Frejo, I. Papamichail, M. Papageorgiou, and E. F. Camacho, "Macroscopic modeling and control of reversible lanes on freeways," *IEEE Transp. on Intelligent Transp. Systems*, vol. 17, no. 4, pp. 948–959, 2015.

[8] K. Ampountolas, J. A. dos Santos, and R. C. Carlson, "Motorway tidal flow lane control," *IEEE Trans. on Intelligent Transp. Systems*, vol. 21, no. 4, pp. 1687–1696, 2020.

[9] Y. Li, S. T. Waller, and A. K. Ziliaskopoulos, "A decomposition scheme for system optimal dynamic traffic assignment models," *Networks and Spatial Economics*, vol. 3, no. 4, pp. 441–455, 2003.

[10] C. F. Daganzo, "The cell transmission model: A dynamic representation of highway traffic consistent with the hydrodynamic theory," *Transp. Research Part B*, vol. 28, no. 4, pp. 269–287, 1994.

[11] M. Duell, M. W. Levin, S. D. Boyles, and S. T. Waller, "System optimal dynamic lane reversal for autonomous vehicles," in *2015 IEEE 18th Int. Conf. on Intelligent Transp. Systems*, pp. 1825–1830.

[12] M. Malekzadeh, I. Papamichail, and M. Papageorgiou, "Linear-Quadratic regulators for internal boundary control of lane-free automated vehicle traffic," *Control Eng. Practice*, vol. 115, 104912, 2021.

[13] K. Zhang, H. Zhang, Y. Mu, C. Liu, "Decentralized tracking optimization control for partially unknown fuzzy interconnected systems via reinforcement learning method," *IEEE Trans. on Fuzzy Systems*; 29(4), pp. 917–26, 2020.

[14] J. Feng, D. Zhao, X.G. Yan and S.K. Spurgeon, "Decentralized sliding mode control for a class of nonlinear interconnected systems by static state feedback," *International Journal of Robust and Nonlinear Control*, *30*(6), pp.2152–2170, 2020.

[15] M. Ikeda, D.D Šiljak, and D.E White, D.E "Decentralized control with overlapping information sets". *Journal of Optimization Theory and Applications*, *34*(2), pp.279–310, 1981.

[16] A. İftar, and Ü. Özgüner, "Contractible controller design and optimal control with state and input inclusion". *Automatica*, *26*(3), pp.593–597, 1990.

[17] Yanumula, V.K., Typaldos, P., Troullinos, D., Malekzadeh, M., Papamichail, I. and Papageorgiou, M., "Optimal path planning for connected and automated vehicles in lane-free traffic". In *2021 IEEE Int. Intelligent Transp. Systems Conference (ITSC)*, pp. 3545–3552.